Quantitative Precipitation Nowcasting: A Lagrangian Pixel-Based Approach

Ali Zahraei [a,*], Kuo-lin Hsu [a,1], Soroosh Sorooshian [a,1], J.J. Gourley [b,2], Valliappa Lakshmanan [c,3], Yang Hong [d,4], Tim Bellerby [e,5]

[a] Center for Hydrometeorology and Remote Sensing (CHRS), The Henry Samueli School of Engineering, Department of Civil and Environmental Engineering, University of California, Irvine, California, E/4130 Engineering Gateway, Irvine, CA 92697
[b] NOAA/National Severe Storms Laboratory, Norman, Oklahoma, 120 David L. Boren Blvd., Rm. 4745, Norman, OK 73072
[c] Cooperative Institute of Mesoscale Meteorological Studies, University of Oklahoma, and NOAA/National Severe Storms Laboratory, Norman, Oklahoma, 120 David L. Boren Blvd., Norman, OK 73072
[d] Department of Civil Engineering and Environmental Science and Atmospheric Radar Research Center, University of Oklahoma, Norman, Oklahoma, 120 David L. Boren Blvd., Rm. 3652, Norman, OK
[e] Department of Geography, University of Hull, Hull, United Kingdom, Cottingham Road, Hull, HU6 7RX, UK

ARTICLE INFO

ABSTRACT

Short-term high-resolution precipitation forecasting has important implications for navigation, flood forecasting, and other hydrological and meteorological concerns. This article introduces a pixel-based algorithm for Short-term Quantitative Precipitation Forecasting (SQPF) using radar-based rainfall data. The proposed algorithm called Pixel-Based Nowcasting (PBN) tracks severe storms with a hierarchical mesh-tracking algorithm to capture storm advection in space and time at high resolution from radar imagers. The extracted advection field is then extended to nowcast the rainfall field in the next 3 hr based on a pixel-based Lagrangian dynamic model. The proposed algorithm is compared with two other nowcasting algorithms (WCN: Watershed-Clustering Nowcasting and PER: PERsistency) for ten thunderstorm events over the conterminous United States. Object-based verification metric and traditional statistics have been used to evaluate the performance of the proposed algorithm. It is shown that the proposed algorithm is superior over comparison algorithms and is effective in tracking and predicting severe storm events for the next few hours.

© 2012 Elsevier B.V. All rights reserved.

1. Introduction and literature review

Nowcasting is referred as forecasting the future state of the atmosphere within a very short time (e.g., 0~3 hr) at a given location. For such short forecast lead times, an effective estimation and extrapolation of existing storms from the current observations (radar and satellite images) is critical (Golding, 1998).

Two primary approaches are used frequently for storm nowcasting depending on the length of prediction and the forecast skill. These approaches are: (1) the application of storm-scale Numerical Weather Prediction (NWP) models which explicitly model the initiation, growth, and dissipation of storms based on the physical modeling of the related atmospheric processes, and (2) "data-driven" extrapolation-based approaches which are storm-tracking and advection-based techniques, with an attempt to predict the evolution of the observed storms (Li et al., 1995; Golding, 1998; Ganguly and Bras, 2003; Bowler et al., 2004; Wilson et al., 2004; Vila et al., 2008; Liang et al., 2010; Liguori et al., 2012; Sokol and Pesice, 2012; Zahraei et al., 2011a, 2011b). Considering the

* Corresponding author at: NOAA-CREST, United States.
E-mail addresses: azahraei@ccny.cuny.edu (A. Zahraei), kuolinh@uci.edu (K. Hsu), soroosh@uci.edu (S. Sorooshian), Jj.Gourley@noaa.gov (J.J. Gourley), lak@vlakshman.com (V. Lakshmanan), yanghong@ou.edu (Y. Hong), T.J.Bellerby@hull.ac.uk (T. Bellerby).
[1] Tel.: +1 949 824 9350; fax: +1 949 824 8831.
[2] Tel.: +1 405 325 6472; fax: +1 405 325 1774.
[3] Tel.: +1 405 325 6569.
[4] Tel.: +1 405 325 3644.
[5] Tel.: +44 1482 466063.

relationship between the length of forecast and specific storm characteristics, such as temporal and spatial scale, both of these methods may be applicable and complementary (Ganguly and Bras, 2003).

As shown in Fig. 1, due to the chaotic characteristic of atmospheric systems, there is always a decaying trend in prediction skill. The relative information content from extrapolation/advection-based methods is best immediately after the storm is observed (within the first 2–3 hr); the relative information content then decreases linearly with time (Austin et al., 1987; Golding, 1998; Lin et al., 2005). For storm-scale prediction, the shorter terms are most likely to be forecasted using extrapolated observations, while the relatively longer-term forecasts (e.g., >3 hr) will likely need to incorporate more dynamics contained in storm-scale NWP models (Ganguly and Bras, 2003).

This study introduces a newly developed algorithm called the Pixel-Based Nowcasting (PBN) algorithm. The PBN technique is being developed to improve short- (or very short) term predictability of severe storms using a high-resolution radar-based rainfall product (Q2).

The following is a brief literature review related to both the NWP and extrapolation-based approaches for Short-term Quantitative Precipitation Forecasting (SQPF) or nowcasting. Then, it will be pursued by methodology, case studies and data, verification and results, and conclusion.

1.1. SQPF and NWP models

During recent years, several NWP models have been used in the United States to make forecasts for short and long periods of time (Wilson et al., 2004). These models have been adapted to predict longer-term atmospheric phenomena with typically coarse spatial and temporal resolutions. As presented in Golding (1998), the NWP model forecasts are relatively sensitive to the initial condition, resolution, and assimilation algorithms, and their capability may not be optimized for very short-term predictions (Fig. 1). Recently, by using a new generation of sensor networks, several different observations have become available in the United States, with sampling frequencies of 1 hr or less. Thus, the application of high-frequency updating of short-term
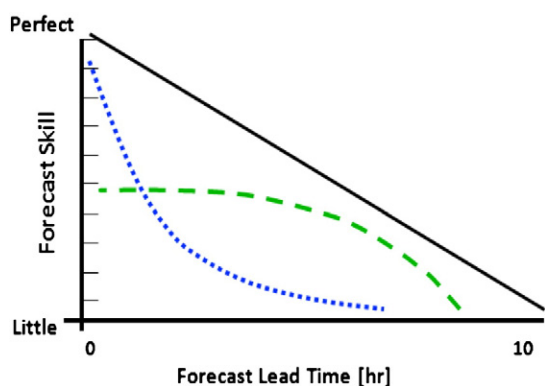

Fig. 1. Representation of the loss of information content in forecasts as a function of lead time. The solid line represents the theoretical limit of predictability, the dashed line indicates NWP models, and the dotted line represents nowcasting methods (Austin et al., 1987).

numerical predictions is facilitated. As a result of the more recent observations, more accurate forecasts are expected (Benjamin et al., 2004).

The first hourly updated, 3-km storm-resolving model, the High-Resolution Rapid Refresh (HRRR) model, was employed recently at the National Oceanic and Atmospheric Administration NOAA/ESRL/GSD. The HRRR model is nested within the Rapid Update Cycle (RUC) and Rapid Refresh (RR). The ability of HRRR in assimilating radar-reflectivity data in the 13-km RUC and upcoming 13-km RR with a version of the Weather Research and Forecasting (WRF) model is considered a significant improvement (Benjamin et al., 2009). Due to its ability to simulate atmospheric physical processes, including convective activities initiation, the HRRR model has found a broad range of applications, particularly for navigation purposes (Wolfson et al., 2008).

Although there have been improvements in the capabilities of NWP models, especially in terms of their contribution in detection of storm-initiation dissipation activities, NWP models still have some limitations for very short-term prediction of smaller-scale storms. For example, Lakshmanan et al. (2009) introduced the position error as a major issue regarding the application of nowcasting methods for the prediction of severe thunderstorms. Therefore, considering that the current research concentrates on short-term predictions (0–3 hrs), as presented in Fig. 1, it is timely to introduce simpler alternative algorithms. As opposed to NWP models, they require much less input data, less computational requirements (cost and time), provide the flexibility of being applicable at the global scale with ever-increasing availability of remotely sensed data, and are more or less as accurate as NWP models.

1.2. SQPF with extrapolation-based models

Some studies have shown that the extrapolation-based algorithms are reasonable nowcasting methods for precipitation (Dixon and Wiener, 1993; Johnson et al., 1998; Germann and Zawadzki, 2002, 2004; Germann et al., 2006; Mueller et al., 2003). Precipitation is an important variable for flash-flood forecasting; reliable nowcasting is in high demand with required temporal and spatial resolution of a few minutes and a few hundred meters (Vasiloff et al., 2007; Vieux and Vieux, 2005). Hence, extrapolation-based nowcasting algorithms using existing remote-sensing information have been used extensively, especially within the first few hours of the occurrence of storm events (Grecu and Krajewski, 2000; Montanari et al., 2006).

A general representation of the extrapolation-based nowcasting system is described below (Grecu and Krajewski, 2000; Laroche and Zawadzki, 1995; Montanari et al., 2006):

$$\frac{\Delta p_t(x,y)}{\Delta t} + U_x(x,y)\frac{\Delta p_t(x,y)}{\Delta x} + V_y(x,y)\frac{\Delta p_t(x,y)}{\Delta y}$$
$$= g[P_t(x,y), \ldots, P_{t-l}(x,y), a(x,y)] + w \qquad (1)$$

in which, $p_t(x,y)$ is the precipitation depth at each location (e.g., the pixel located on (x,y) at time t), $\mathbf{U}_x$ (velocity in the x direction; West–east), and $\mathbf{V}_y$ (velocity in the y direction; North–south) are advection-field components of the rainfall field for storms located on (x,y). g is a function of parameters a that needs to be estimated using $(P_t, \ldots, P_{t-l})$ rainfall rate in current and previous time steps, and w is the noise element.

According to Eq. (1), the rainfall-depth variation at time t and at (x,y), $\Delta p_t(x,y)$ would be a function of two parallel processes. The second and third terms on the left-hand side of Eq. (1) introduce a Eulerian process, in which the storm is moving in the Eulerian reference frame. The storm variation is a result of the advection vectors of $\mathbf{U}_x$, $\mathbf{V}_y$. In addition, the function g represents a dynamical Lagrangian process in which a future storm's intensity is a result of its historical changes in a Lagrangian reference frame that travels along the storm path (Grecu and Krajewski, 2000). Considering a storm in the smallest possible unit (pixels), Eq. (1) presents a pixel-based definition of nowcasting in which the storm moves forward pixel-by-pixel.

As suggested by Austin and Bellon (1974), a nowcasting algorithm should consist of a tracking and forecasting process. Several attempts to improve the trackability of the storms' movements have been made. Some investigators have proposed approaches to track and forecast thunderstorms with the highest possible resolution (Eq. (1): spatial resolution in the scale of each pixel) (Tuttle and Foote, 1990; Grecu and Krajewski, 2000; Germann and Zawadzki, 2002; Ridal et al., 2010). Two particular classes of algorithms have been used to estimate storm velocity from two consecutive images. The first approach is based on the maximum correlation between two successive images (Smythe and Zrnic, 1983; Tuttle and Foote, 1990; Laroche and Zawadzki, 1995). The second approach assumes that changes in the first image (e.g., advection) result in the second image. The advection field is then estimated by minimizing the difference between the reshaped first image and the second image (Germann and Zawadzki, 2002, 2004; Turner et al., 2004). For example, Germann and Zawadzki (2002) estimated the echo motion field by utilizing the Variational Echo Tracking (VET) algorithm to retrieve 2-D advection-field components including: $\mathbf{U}x$ (velocity component in the x direction), $\mathbf{V}y$ (velocity component in the y direction), by minimizing a large-scale nonlinear cost function. Regardless of the complexity of solving a large-scale nonlinear optimization problem, the VET algorithm is sensitive to the first guess (Laroche and Zawadzki, 1995).

1.3. Necessity for new tracking and nowcasting algorithms

Many radar-based wind-retrieval algorithms employ template-matching algorithms to estimate inter-image displacement (Leese et al., 1971). These methods compare the patterns of pixels within a small window in a given image with similar patterns at potential corresponding locations in the subsequent image. A similarity measure, such as maximum correlation, can identify the most matching locations. However, the correlation surfaces associated with the search algorithms frequently display diffuse or multiple optima. Similarly, the simple template-matching algorithm operates based on window translations which are relatively incapable of accommodating feature rotation and deformation (Bellerby, 2006).

To overcome the aforementioned problem of simple template-matching algorithm, several techniques impose smoothness criteria on the displacement field. It is also suggested to adopt a hierarchical representation of the displacement field in which each feature motion is considered as the sum of smoothly varying trends identified at relatively coarse spatial resolution and smaller magnitude local correction derived at progressively higher spatial scales (Bergen et al., 1992). It is also possible to couple hierarchical-tracking approaches with mesh-based models of image deformation. Mesh models provide a piecewise representation of the displacement field in which displacement is defined over the nodes of a mesh and interpolated within each mesh element (Wang and Lee, 1996). In this article, a newly developed hierarchical storm-advection algorithm based on the topological transformation of a quadrilateral mesh is implemented (Bellerby, 2006). This algorithm is a computationally efficient technique to capture movements and rotations of storms. The algorithm has shown promising performance in tracking storms (Behrangi et al., 2010).

The proposed tracking algorithm, along with the projection scheme, is able to track the advection and rotation of small scale, fast-moving thunderstorms that could not be necessarily predictable using the current algorithms. The proposed PBN predicts both storm advection and its dynamical features (e.g., rainfall-intensity changes). The PBN algorithm could track and forecast relatively small-scale severe storms that have significant importance regarding their associated catastrophic phenomena, such as tornados and severe rainfall.

The newly proposed PBN technique will be compared to two existing algorithms including: WCN and PER. One current state-of-the-art of nowcasting is called Watershed-Clustering Nowcasting (WCN) in the current research. The WCN, developed by the National Severe Storm Laboratory (NSSL) and the University of Oklahoma, is part of the Warning Decision Support System-Integrated Information (WDSS-II) system (Lakshmanan et al., 2009). The algorithm is computationally efficient and effective for the identification and tracking of severe thunderstorms. The algorithm has a few consecutive steps, including smoothing, quantization, transformation, immersion simulation, and affecting the scale. The algorithm proposes a watershed transform model where the storm objects are defined as salient if they can pass size criteria instead of considering watershed depth. Therefore, it is not necessary to define different thresholds and watershed depth criteria. The algorithm uses the cost-function optimization problem to track storm objects (Dixon and Wiener, 1993). PER is the PERsistency algorithm which assumes there is a frozen situation that storm does not change.

The main contribution of this paper can be summarized as follows: (1) implementing a newly developed pixel-based tracking algorithm to track each rainy pixel advection, which improves the predictability of smaller-scale severe rainfall events.; (2) extract storm-advection field and dynamic-evolution features based on Step (1); (3) storm projection (extrapolation) including both storm advection and evolution (e.g., rainfall-intensity change); and (4) comparison with other techniques. Being simple and not a computationally time-consuming algorithm, the PBN is offered to provide a relatively accurate initial forecast for severe events in short-term lead time.

2. Methodology

2.1. Pixel-Based Nowcasting (PBN) algorithm

Thunderstorms usually have relatively small-scale high-rainfall cores that should be predicted accurately. Regardless of
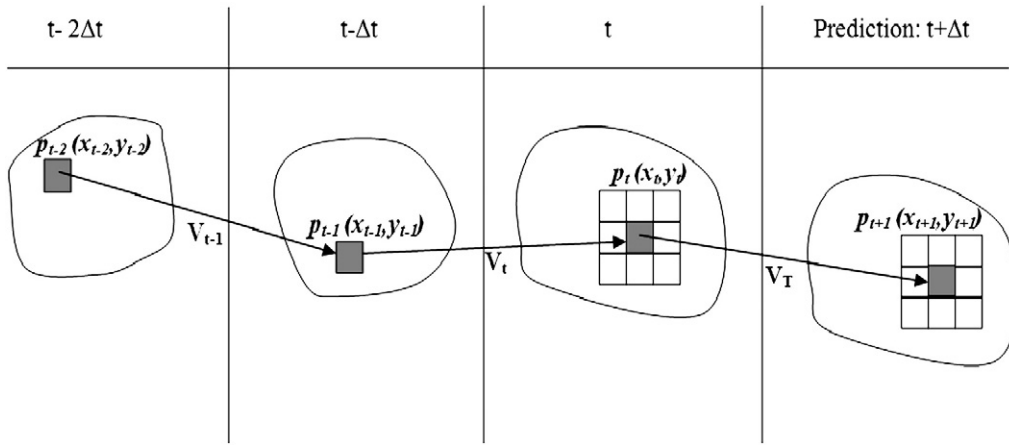
Fig. 2. Proposed PBN algorithm, V_{t-1}: The specified darker pixel advection vector between $t-2\Delta t$ and $t-\Delta t$; V_t: pixel advection vector between $t-\Delta t$ and t; V_P: predicted advection as a function of V_{t-1} and V_t for the darker (central) pixel; V_T: average predicted advection vectors of all V_P for nine pixels (window 3×3) centered on the darker pixel $V_T = \sum V_p/9$.

their sizes and relatively short lifetimes, the advection-based nowcasting algorithm should enhance the prediction of the storms' future positions. Therefore, the PBN algorithm forecasts storms associated with intensive rainfall more accurately using a pixel-based storm-tracking process to catch each storm dynamic advection process using radar imagery, and then an extrapolation/nowcasting step that provides the dynamic evolution of pixel position and precipitation intensity from the current to the future time steps. The PBN uses the high-resolution pixel-based tracking algorithm adapted to track rainy pixels (pixels more than 0.4 mm/hr). The tracking algorithm finds the corresponding location of each rainy pixel in the previous time step(s). After tracking each rainy pixel in time, the corresponding advection velocity and evolution trend (rainfall-intensity change) for each pixel will be known. The extracted features can be used to project the storm. This algorithm is summarized in Eqs. (2)–(5):

$$\text{Predicted rain rate at } t + n\Delta t = p_{t+n\Delta t}(x_{t+n\Delta t}, y_{t+n\Delta t})$$
$$= \min\{p_t(x_t, y_t) + n\Delta P; \ Threshold\} \quad (2)$$

$$\text{Predicted location}: (x_{t+n\Delta t}, y_{t+n\Delta t}) = (x_t, y_t) + n\Delta(x_t, y_t) \quad (3)$$

$$\text{Predicted displacement from } t \text{ to } t+1 : \Delta(x_t, y_t)$$
$$= f_1\{(x_t, y_t), (x_{t-\Delta t}, y_{t-\Delta t}), (x_{t-2\Delta t}, y_{t-2\Delta t}), \ldots\} \quad (4)$$

$$\text{Predicted rainfall trend}: \Delta P$$
$$= f_2\{p_t(x_t, y_t), p_{t-1}(x_{t-\Delta t}, y_{t-\Delta t}), p_{t-2}(x_{t-2\Delta t}, y_{t-2\Delta t}), \ldots\} \quad (5)$$

in which $p_{t+n\Delta t}$ $(x_{t+n\Delta t}, y_{t+n\Delta t})$ (intensity/time) is the predicted rainfall rate for the pixel located on $(x_{t+n\Delta t}, y_{t+n\Delta t})$ in time $t+n\Delta t$ (t: the current time; if n=1, $t+\Delta t$: one time-step prediction, each time step=time interval between two consecutive radar imageries), and p_t (x_t, y_t) is the precipitation rate at time step t corresponding to the location (x_t, y_t). The pixel-based tracking algorithm finds the corresponding location of each rainy pixel in the previous time steps with time interval Δt; for example, $p_{t-\Delta t} (x_{t-\Delta t}, y_{t-\Delta t})$ at time $t-\Delta t$ is the pixel that corresponds to $p_t (x_t, y_t)$ at time t. The functions f_1 and f_2 represent a dynamical Lagrangian

process in which the reference frame moves with each pixel. The function f_1 is used to estimate each pixel advection. n is the prediction step. The PBN algorithm provides predictions every 10 min up to 180 min ($n=1, 2, \ldots, 18$).

The advection-based displacement $\Delta(x_t, y_t)$ is a function of each specific pixel location in previous time step(s). The PBN
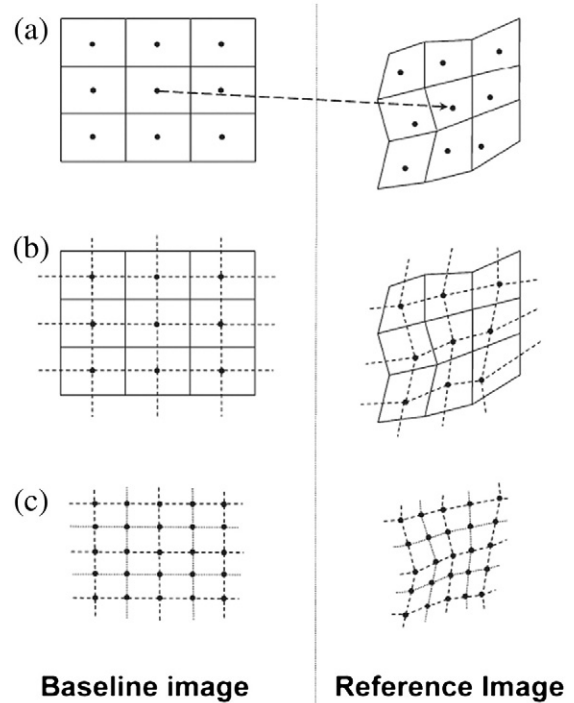

Fig. 3. Representation of the mesh-based tracking algorithm. (a) Image template matching to locate the position in the reference image which most closely corresponds to the center of each baseline mesh. (b) Mesh replacement by meshes of baseline centers and corresponding optimal matching locations. (c) Mesh interpolation. (Bellerby, 2006, used with permission).
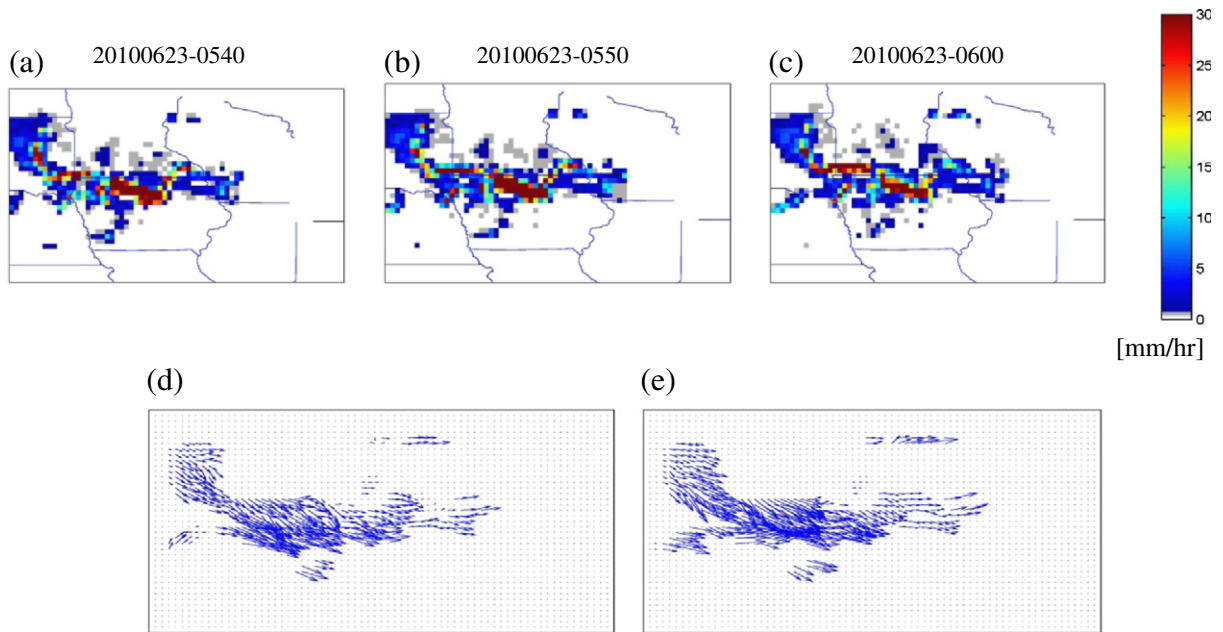
Fig. 4. Three consecutive radar images ($\Delta t = 10$ minutes; Spatial resolution ~20 km): (a) 20100623–0540, (b) 20100623–0550, (c) 20100623–0600, (d) extracted advection field between (a) and (b), and (e) extracted advection field between (b) and (c), (Rainfall Unit = mm/hr).

assumes that the rate of rainfall $p_{t+\Delta t}$ $(x_{t+\Delta t}, y_{t+\Delta t})$ is a function of the current and previous time steps(s). Similarly, the function f_2 is used to estimate Δp based on previous time steps. The Δp is the rainfall trend for each specific rainy pixel. In growing convective storms, Δp can be a significant positive quantity. In order to avoid unreasonable values, a threshold is set to limit the maximum values each rainy pixel might be assigned to.

According to Eqs. (6)–(8) and Fig. 2, f_1 and f_2 are used to predict storm advection and intensity, respectively.

$$
\begin{aligned}
\Delta(x_t, y_t) &= f_1\{(x_t, y_t), (x_{t-\Delta t}, y_{t-\Delta t}), (x_{t-2\Delta t}, y_{t-2\Delta t})\} \\
&= f_1[V_t(x_t, y_t)\Delta t \ ; \ V_{t-1}(x_{t-\Delta t}, y_{t-\Delta t})\Delta t] = \\
&= V_p \times \Delta t = mean(Dist_1 ; Dist_2)
\end{aligned}
\tag{6}
$$

$$
Dist_1 = \left((x_t - x_{t-\Delta t})^2 + (y_t - y_{t-\Delta t})^2\right)^{0.5} \ ; \quad Dist_2
$$
$$
= \left((x_{t-2\Delta t} - x_{t-\Delta t})^2 + (y_{t-2\Delta t} - y_{t-\Delta t})^2\right)^{0.5}
\tag{7}
$$

$$
\Delta P = f_2\{p_t(x_t, y_t), p_{t-1}(x_{t-\Delta t}, y_{t-\Delta t}), p_{t-2}(x_{t-2\Delta t}, y_{t-2\Delta t})\} =
$$
$$
[\{p_t(x_t, y_t) - p_{t-1}(x_{t-\Delta t}, y_{t-\Delta t})\} + \{p_{t-\Delta t}(x_{t-\Delta t}, y_{t-\Delta t}) - p_t\}/2
$$
$$
-2\Delta t(x_{t-2\Delta t}, y_{t-2\Delta t})\}
\tag{8}
$$

The V_{t-1} vector corresponds to advection for one specific pixel $p_{t-2\Delta t}$ $(x_{t-2\Delta t}, y_{t-2\Delta t})$ at time $t-2\Delta t$ moved to $p_{t-\Delta t}$ $(x_{t-\Delta t}, y_{t-\Delta t})$ at time $t-\Delta t$. The V_t represents the advection field between time $t-\Delta t$ and t. As soon as the advection vectors for the three time steps are known, a function f_1, which can be a

Table 1
Information for ten storms/events, including time, length, and states damaged by the storm. The fifth column shows if the thunderstorms caused fatality damage, the sixth column shows if the damage exceeded more than 1 million dollars, and the last three columns show if the thunderstorms had severe winds, flash flooding, and/or tornados (source: National Climate Data Center).

| Event	Time [mm/dd/yy]	Length [hr]	States	Death	Damage > 1 M	Severe Wind	Flash Flood	Tornado
1	05/08/09	18	KS, MO, KY, VA	Yes	Yes	Yes	Yes	Yes
2	06/[09–10]/09	18	KS, MO	No	No	Yes	Yes	Yes
3	06/[13–14]/10	24	OK, KS	Yes	Yes	Yes	Yes	Yes
4	06/[22–23]/10	21	NE, SD, IA, WI	No	Yes	Yes	Yes	Yes
5	08/[13–14]/10	12	KS, MO, IL	No	No	Yes	Yes	No
6	09/[13–14]/10	25	NE, IO, KS, MO, OK, AR	No	No	Yes	Yes	Yes
7	06/[18–19]/09	27	NE, IA, IL, IN, KY,NC, GA	Yes	Yes	Yes	Yes	Yes
8	07/[24–25]/09	24	MN, IA, WI, IL, IN	No	Yes	Yes	Yes	Yes
9	08/08/09	18	MN, WI, IL, IN, MI, IA	Yes	Yes	Yes	Yes	Yes
10	08/[25–26]/09	19	CO, KS, NE	No	No	Yes	Yes	No
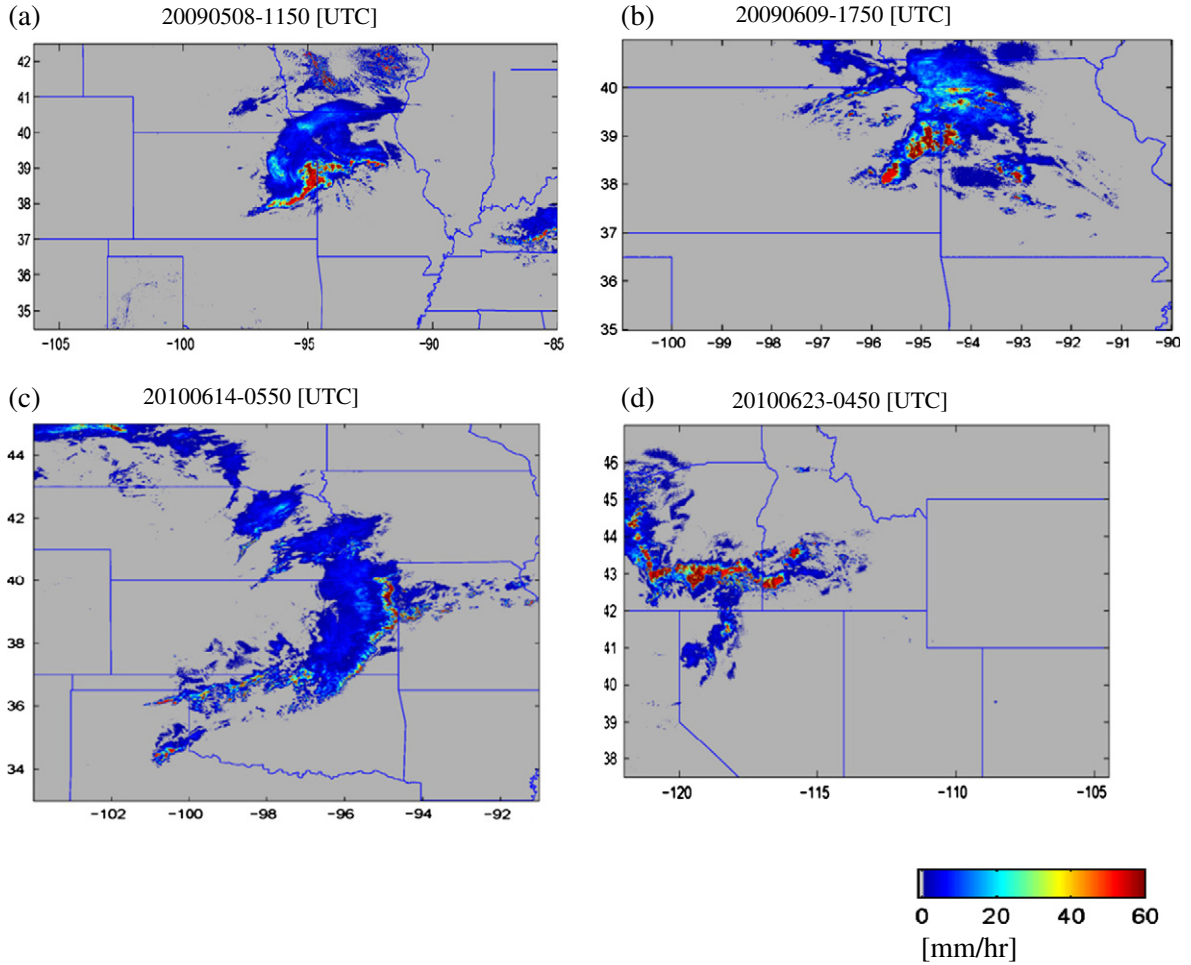
Fig. 5. Four selected severe storms: (a) Event 1:20090508–1150 [UTC], (b) Event 2: 20090609–1750 [UTC], (c) Event 3: 20100614–0550 [UTC], and (4) Event 4: 20100623–0450 [UTC], along with the spatial domain in which the storms produced significant rainfall (Rainfall Unit = mm/hr).

linear combination of both V_{t-1} and V_t, has been applied. Δt is the time interval between two consecutive time steps. PBN uses an average of two advection vectors (V_P) as a reasonable estimation for storm extrapolation in a Lagrangian reference frame (Fig. 2).

The current time step t and the previous time step t-Δt could provide the advection field of each pixel. Nevertheless, PBN applies three time steps: t, t-Δt, and t-$2\Delta t$. Three previous successive time steps provide two advection fields, including $V_{t-\Delta t}$ and $V_{t,}$ which are able to capture both the direct and rotational movement of each storm.

The PBN algorithm applies both the advection field (V_P) and the storm evolution (rainfall-intensity changes). In Eqs. (6)–(8), the function f_2 uses three previous time steps, t, t-Δt, and t-$2\Delta t$, to extract Δp. Function f_2 is used to predict the rate of rainfall $p_{t+\Delta t}$ ($x_{t+\Delta t}$, $y_{t+\Delta t}$) for time $t+\Delta t$ at each rainy pixel based on the rainfall rate of that pixel in the last three time steps. The f_2 is a function of the rainfall-rate variation for a pixel located at p_{t-1} ($x_{t-\Delta t}$, $y_{t-\Delta t}$) time t-Δt moved to p_t (x_t, y_t) at time t and the variation between time t-Δt and t-$2\Delta t$. For each pixel, the average of these two trends

has been used for intensity prediction at $t+\Delta t$. The same trend can be applied for time steps $t+2\Delta t$, $t+3\Delta t$, etc., until the rainfall rate reaches some predefined maximum threshold. If the trend is negative, there will be also a minimum threshold that is equal to zero rainfall.

Using Δp and V_p, the PBN algorithm projects the storm's length of prediction up to 3 hrs (180 min). The PBN algorithm updates predictions every 10 min. According to Eqs. (6)–(8), similar advection velocity (V_p) and the intensity-changes trend (Δp) for the first time step ($t+n\Delta t$; $n=1$) will be applied for the next time steps ($t+n\Delta t$), where ($n=2, 3,..., 18$).

Given the fact that the proposed PBN is a Lagrangian dynamic model, each pixel should be extrapolated in a Lagrangian reference system. The V_p, the average of $V_{t-\Delta t}$ and V_t, is the advection vector for a specified pixel between t-$2\Delta t$, t-Δt, and t-Δt, t, respectively (Fig. 2). To reduce the projection noise and fill probable discontinuities, a low-pass spatial filter (3×3) is applied. Each rainy pixel will be considered as a center of a 3×3 window of pixels, and the advection field for the window (V_T) will be an average of the advection fields

Table 2
The contingency table, F = Forecast, O = Observation, Tr is the predefined rainfall threshold.

Event	Condition
Success	F > Tr and O > Tr
False Alarm	F > Tr and O < Tr
Failure	F < Tr and O > Tr
Correct Negative	F < Tr and O < Tr

V_p for pixels inside the window. A larger filter could not be applied effectively for the prediction of small-scale storms.

For every event, there is a moving window traveling with each specific storm throughout the storm lifecycle. The dynamic window moves with the storm in such a way that it is always concentrated on that storm. Because this is an event-based study to evaluate the PBN algorithm, using a dynamic window creates less error. The pixel-based algorithm is updated every 10 min as new radar imagery exists using three consecutive time steps (t = current time) and (t-Δt, t-$2\Delta t$ = previous time steps).

The pixel-based tracking algorithm possesses a template-matching characteristic that operates based on the maximum correlation between meshes in two consecutive images. As opposed to the other tracking techniques, the PBN algorithm does not require any nonlinear programming, which is computationally time consuming and erroneous. Two consecutive images should have a suitable time interval to correctly retrieve the rainfall-advection field. The current study shows that $\Delta t = 10$ min is reasonable for retrieving the advection field.
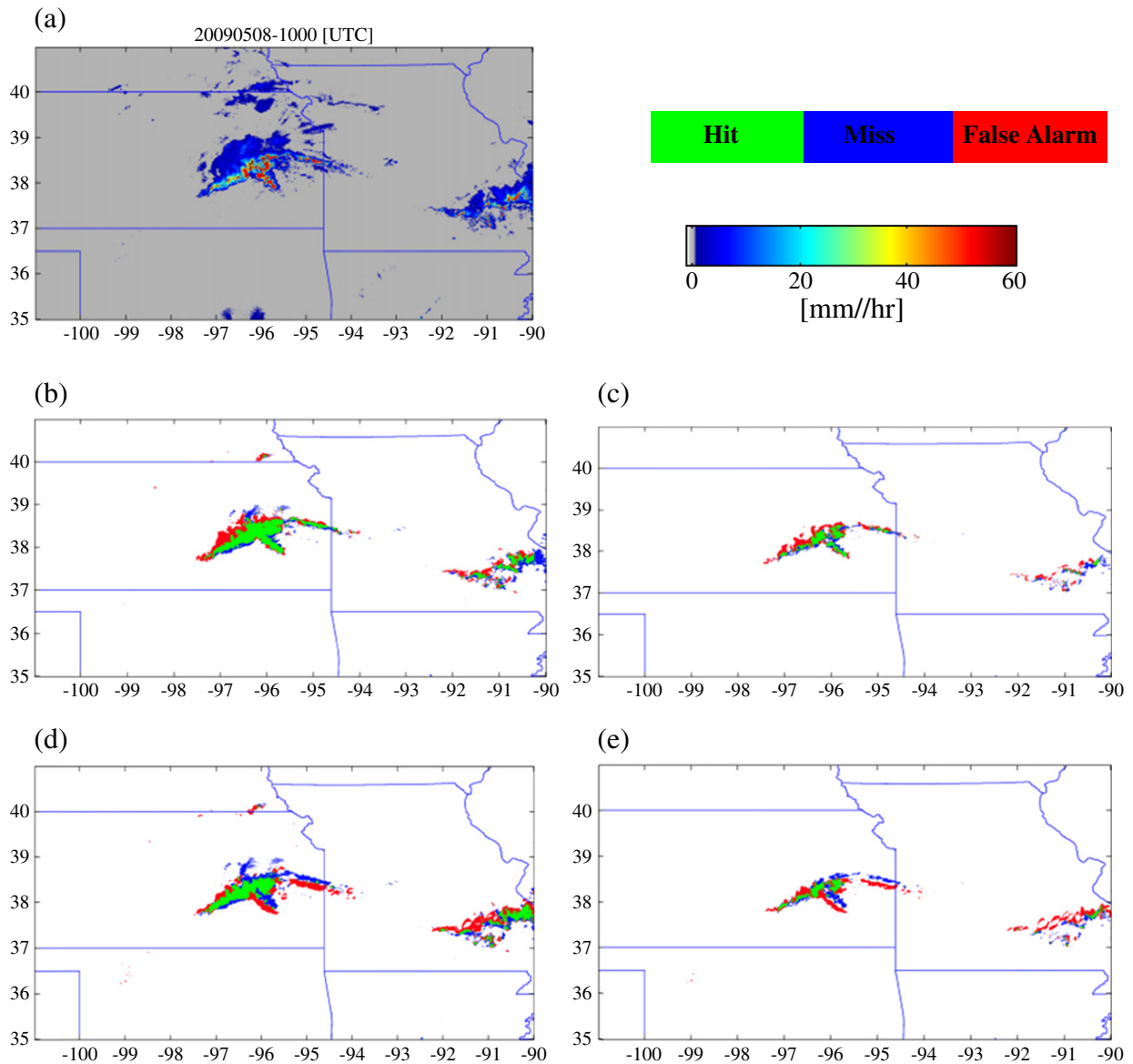

Fig. 6. (a) Event 1 on 8 May 2009, 10:00 AM [UTC] observation, Q2 1 [km]. (b, c) PBN + 30 [min] prediction and 5 and 20 [mm/hr] thresholds. (d, e) WCN + 30 [min] prediction with 5 and 20 [mm/hr] thresholds (Rainfall Unit = mm/hr).

Table 3
PBN and WCN algorithms, POD and FAR, for the event shown in Fig. 6, using two rainfall thresholds 5 [mm/hr] and 20 [mm/hr].

Nowcasting Rain: [mm/hr]	POD	FAR	Nowcasting	POD	FAR
PBN, Rain>5	53	51	PBN, Rain>20	41	62
WCN, Rain>5	44	61	WCN, Rain>20	30	77

The PBN algorithm tracks the storm behavior during the past 20 (=2Δt) min, the historical knowledge of each particular storm will be used to extrapolate storms (Grecu and Krajewski, 2000).

The proposed algorithm for storm tracking and nowcasting is discussed below.

2.2. Pixel-based storm tracking

There have been some efforts to combine mesh-based and hierarchical techniques in order to enable better tracking of small-scale complex features, such as scaling, rotation, and shear (Toklu et al., 1996; Bergen et al., 1992). This paper applies a version of a newly developed pixel-based advection algorithm to identify the corresponding location of each rainy pixel in the previous subsequent image(s) (Bellerby, 2006). The tracking algorithm operates at multiple spatial resolutions, initially estimating advection vectors at a very coarse resolution and then spatially refining the field down to a pixel level. It is thus designed to generate a spatially continuous and smooth vector field that does not suffer from discontinuities at template boundaries. Moreover, the tracking algorithm is robust with respect to sparse precipitation fields, and the initial tracking phase matches large templates and can robustly estimate the movement of a sparse field. The finer-scale stages of the tracking scheme are limited to rainy areas and constrained by the initial phase in a manner that prevents false matches.

In fact, the multiscale nature of the tracking algorithm could make it relatively robust with respect to the skewness problem and matching high precipitation values that has a disproportionate effect on the overall pattern match. However, to minimize the tracking algorithm probable sensitivity to the data structure, the PBN algorithm applies, smoother log transformed data field. The current study uses $log(R)$; in which R is the rain rate.

Then, the applied algorithm uses coarse-resolution quadrilateral meshes fully draped over the first image (time=t-Δt) called the Baseline image, and the subsequent one is called the Reference image (time=t). A rectangular-window, translational, correlation-matching procedure then deforms the rectangular mesh covering the preceding image into a convex quadrilateral mesh, optimizing the correspondence between the two images at and around equivalent mesh nodes. The meshes over both images are interpolated to twice their previous spatial resolution, and the correlation-matching procedure is repeated, this time taking into account local
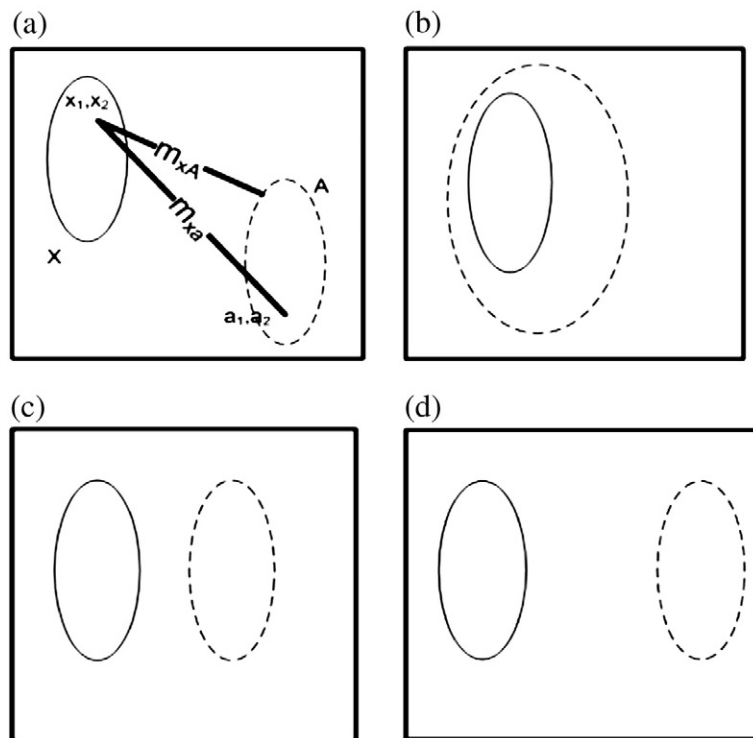

Fig. 7. The solid oval represents observation and the dashed oval represents forecast. (a) Euclidean metric function between points and between one point and a bounded set; (b) dist DV=0, dist OV≠0; (c, d) [dist DV (e)<dist DV (f)] and [dist $_{OV}$ (e)=dist $_{OV}$ (f)≠0] (from Zhu et al., 2011).

distortions represented by the non-rectangular mesh. Incorporating these local distortions enables the tracking algorithm to accommodate rotational and shear effects, in addition to translations. The interpolation and matching stages iterate until the mesh resolutions reach the original image (Q2 radar data) resolution. Later iterations of the algorithm interpolate both images to four times their original spatial resolution using bi-cubic splines before starting the correlation-matching procedure. At the end of the final iteration, each rainy pixel location (x_t, y_t) in the main image is associated with an equivalent location $(x_{t-\Delta t}, y_{t-\Delta t})$ in the same storm in the preceding image. Additionally, the algorithm is capable of deriving the reverse mapping, relating each pixel in the preceding image to an equivalent location in the current image from the same pair of final meshes without re-running the tracking procedure (Bellerby, 2006). The 2-D rainfall-advection algorithm is computationally efficient and has shown to be both robust in the presence of image rotation and shear (Zahraei et al., 2012, submitted for publication). Fig. 3 illustrates the key stages of the procedure for an arbitrary iteration (Bellerby, 2006), including:

(1) A correlation-based, template-matching algorithm is used to relate the closest point of each Reference mesh to the center point of each Baseline image mesh.

(2) The Reference and Baseline meshes are replaced based on central and closest match points identified in Step 1.

(3) Adjacent nodes in the new Reference mesh are checked for consistency. Nodes which are inconsistent are replaced by alternative cross-correlation matches.

(4) Concave quadrilateral meshes/elements in the Reference mesh will be removed.

The current study applies the extracted rainfall advection fields to predict storm advection and intensity.

Fig. 4 illustrates the application of the pixel-based tracking algorithm to track a severe storm in three consecutive radar images. Fig. 4d and e show that the tracking algorithm could successfully track the storm advection in the pixel scale.

3. Data and Case Studies

The next step involves the application and testing (verification) of the proposed PBN algorithm presented above. For this purpose, radar observations are used. Radar images have been used frequently in detecting severe storms. For this study, the Q2 radar-based quantitative precipitation estimation data set with
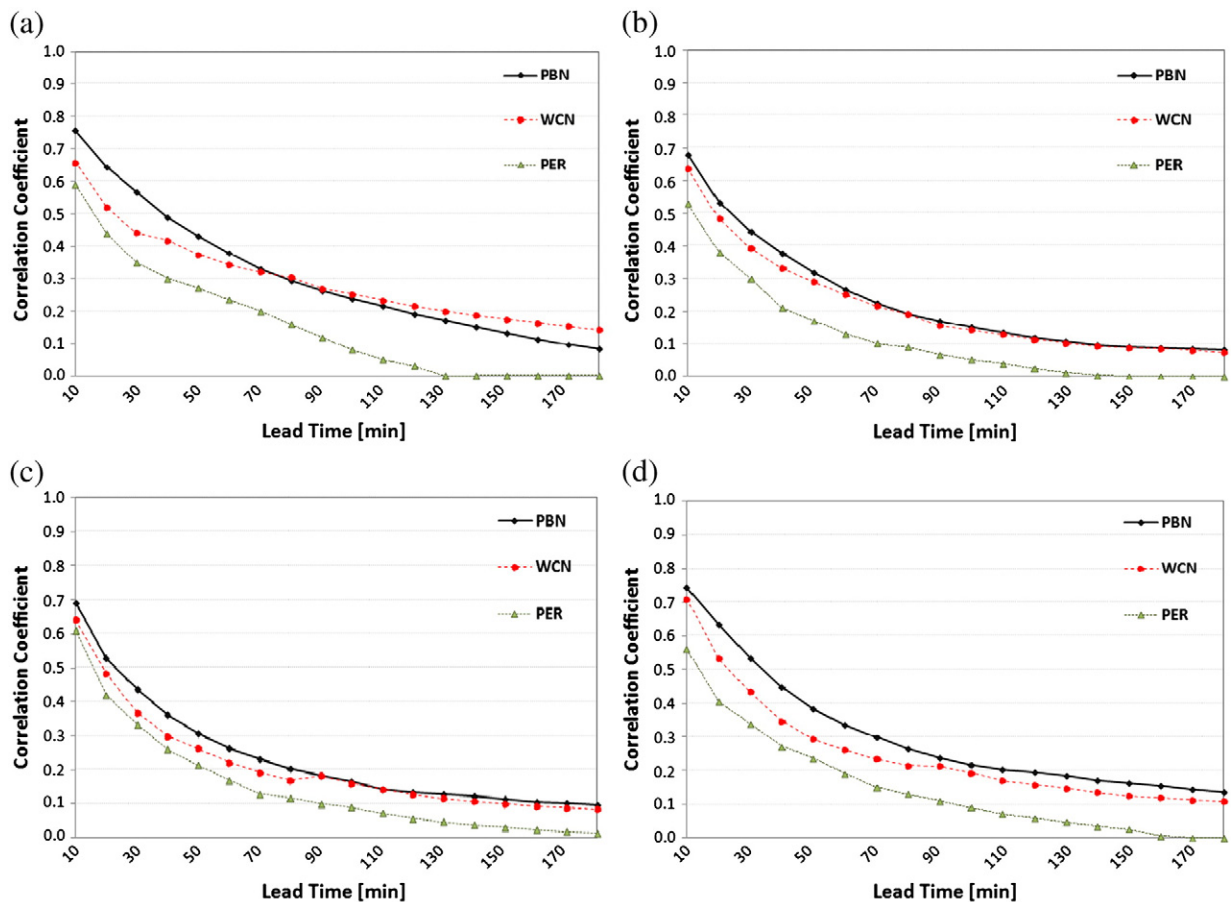

Fig. 8. Correlation Coefficient (C) vs. lead time [min], in which the larger values represent better prediction: (a) Storm 1, (b) Storm 2, (c) Storm 3, and (d) Storm 4. Three models: PBN, WCN, and PER.
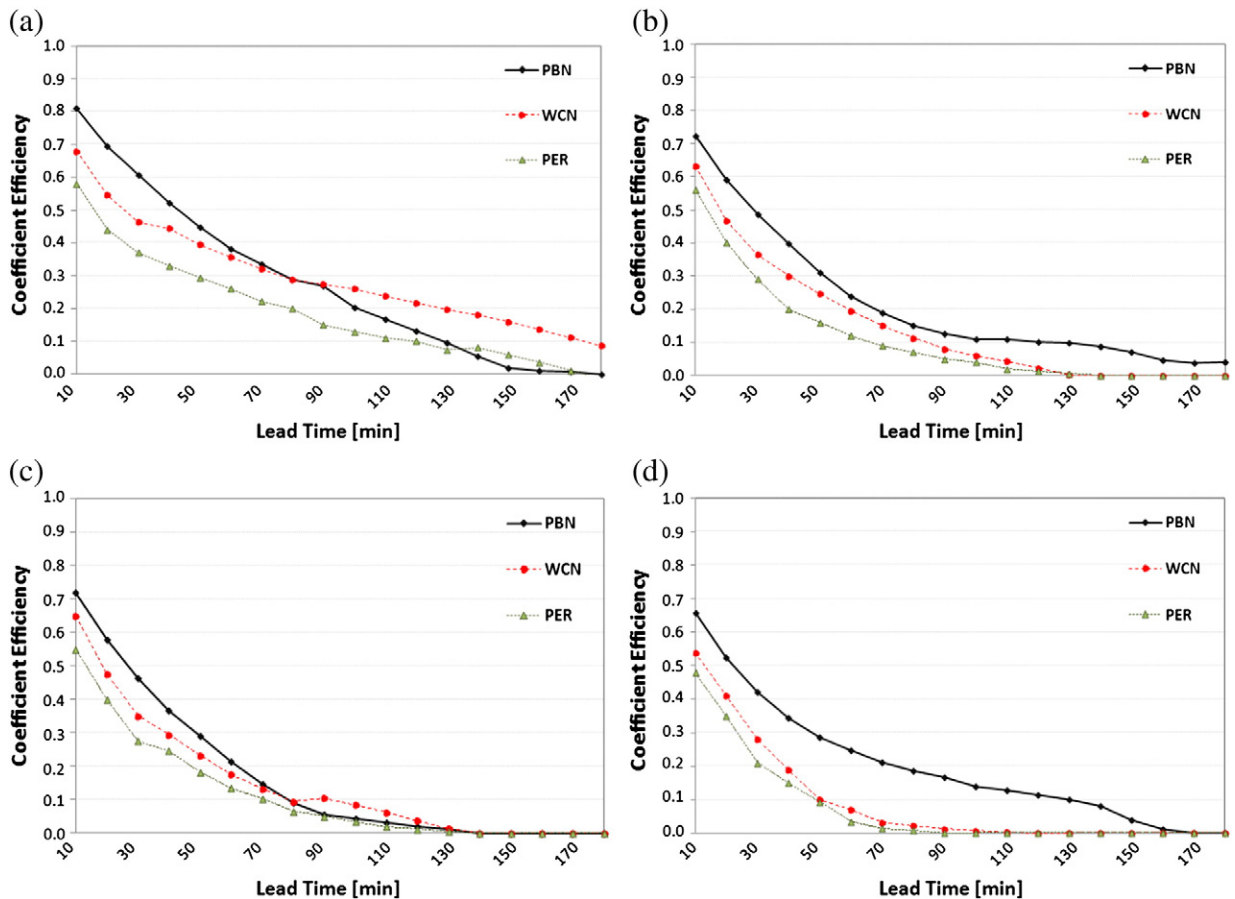
Fig. 9. Coefficient of Efficiency (E), $-\infty < E < 1$, vs. lead time [min], in which the larger values represent better prediction: (a) Storm 1, (b) Storm 2, (c) Storm 3, and (d) Storm 4. Three models: PBN, WCN, and PER.

0.01° spatial and 2.5-5-min temporal resolution over the entire conterminous U.S. (CONUS) produced by the NOAA-NSSL is used (Vasiloff et al., 2007). This study focuses on the application of the radar-based rainfall products Q2 in nowcasting. The driving hypothesis is that the selected Q2 is an improved radar data set which has significantly filtered the effect of contaminants, such as insects, anomalous propagation, and ground clutter (Lakshmanan et al., 2007). This study applies a resolution of 1 km for each 10 min and evaluates the use of the proposed PBN algorithm to predict precipitation in storm-scale or mesoscale atmospheric phenomena. Ten relatively severe storm events within the CONUS area are selected based on the reported severe winds, flash floods, or tornados that they have produced (National Climatic Data Center; ncdc.noaa.gov). Table 1 shows the studied events. The aforementioned events occurred during 2009 or 2010, with lifecycles not exceeding more than 25–30 hrs. All of the events caused major property damage and/or human fatalities (National Climatic Data Center; ncdc.noaa.gov). Relatively speaking, the storm events are small-scale, fast-moving thunderstorms with typically complicated structures. Although there has been a comprehensive study on all events, four storms will be examined more closely (Fig. 5) due to some specific features. The first storm (shown in Fig. 5a) is a small-scale, fast-moving thunderstorm. Its complex structure makes it difficult to segment and track by

using current techniques. The second storm shown (Fig. 5b), which starts with a localized convective structure, has broken into several smaller parts that move, rotate, and disappear very fast in a few hours. The storm produces a significant amount of rainfall. The third event (Fig. 5c) is a very unique storm in terms of its being nearly stationary and slow moving. This storm produced more than 250 mm of rainfall in approximately 6 hr over Oklahoma City, OK, resulting in flash flooding in the urbanized area. The fourth storm (Fig. 5d) is a significant event that produced severe rainfall and caused flooding in the area. Despite its large-scale structure, the storm is generated from some smaller, very fast-moving storms. This storm moves hundreds of kilometers in a matter of several hours.

4. Verification and Results

The proposed PBN approach is compared with two nowcasting algorithms that have been presented in the literature (Montanari et al., 2006). Both of these algorithms are based on Eq. (1) and are described below.

4.1. Eulerian-Persistence Model (EPM)

The Eulerian-Persistence Model (EPM) or a Persistency (PER) model assumes that the future rainfall field is equal to
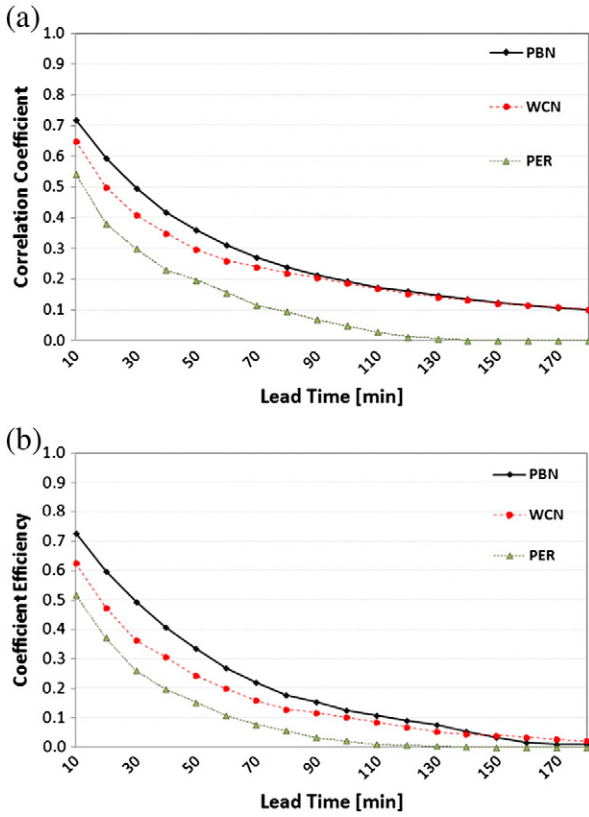
(a)

(b)

Fig. 10. (a) Correlation Coefficient (C) average for ten storms vs. lead time [min]. (b) Coefficient of Efficiency (E) average for ten storms vs. lead time [min], both PBN and WCN algorithms, in which the larger values represent better prediction. Three models: PBN, WCN, and PER.

the last available scan in which all terms in Eq. (1) are eliminated, except:

$$\frac{\Delta p_t(x,y)}{\Delta t} = 0 \qquad (9)$$

The PER model is used as a benchmark to evaluate prediction skill. The PER model assumes that the storm
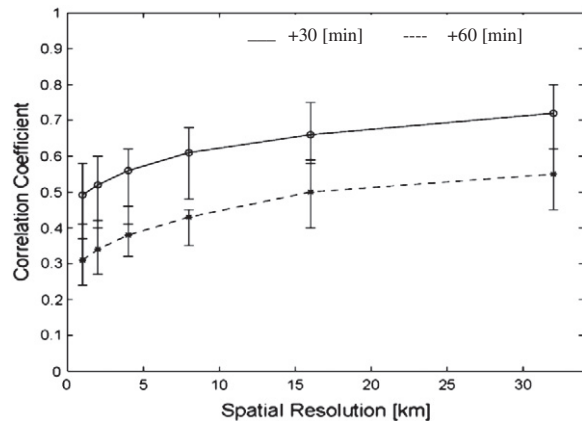

Fig. 11. The Correlation Coefficient (C) vs. different spatial resolution [km] for different lead times [min] using the PBN algorithm. The coarser resolution has better prediction skill.

movement is negligible and assigns the same forecasted rainfall intensity as the last available storm imagery. The PER model is considered to be a reasonable short-term prediction for stationary storms.

4.2. Lagrangian-Persistence Model (LPM)

Advection is a key element in storm movement and nowcasting (Austin and Bellon, 1974). The Lagrangian persistence model considers the storm advection while ignoring the rainfall dynamic changes. The equation can be rewritten as:

$$\frac{\Delta p_t(x,y)}{\Delta t} + U_x(x,y)\frac{\Delta p_t(x,y)}{\Delta x} + V_y(x,y)\frac{\Delta p_t(x,y)}{\Delta y} = 0 \qquad (10)$$

It is documented that a uniform U_x and V_y over the whole study domain might be a reasonable approximation for larger-scale storms (Pegram and Clothier, 2001a, 2001b; Seed, 2003). The LPM model, called WCN in the current study, is used for comparison with the proposed PBN algorithm (Lakshmanan et al., 2009). All nowcasting algorithms, including WCN, proposed PBN, and PER, have been implemented to predict the rainfall rate in the next 3 hr.

4.3. Verification procedure

A quantitative assessment commonly referred to as model verification is required to assess the degree to which the prediction and observation match each other. The model verification techniques usually use a pair-wise comparison of prediction and observation values. Given the spatial nature of radar observations, verification methods capable of quantifying the model performance over a prescribed domain are needed.

There are two approaches available for spatial verification, namely pixel-based and object (feature)-based methods. The pixel-based methods utilize a point-to-point or pixel-to-pixel comparison between prediction and observation, while the object-based methods typically model storms as separate objects. Because each of these verification methods has some limitations, this study uses both approaches.

4.3.1. Pixel-to-pixel based verification methods

Four performance measures are used for pixel-to-pixel verification of PBN. They include coefficient of Correlation (C), coefficient of Efficiency (E), Probability of Detection (POD), False-Alarm Ratio (FAR), and Odds ratio. They measure the agreement between forecast (F) and observation (O) (Legates and McCabe, 1999). The coefficient of correlation C is defined as:

$$C = \frac{\sum\limits_{i=1}^{N}(O_i - \bar{O})(F_i - \bar{F})}{\left(\sum\limits_{i=1}^{N}(O_i - \bar{O})^2\right)^{0.5}\left(\sum\limits_{i=1}^{N}(F_i - \bar{F})^2\right)^{0.5}} \qquad (11)$$

where the bar represents the average values, and N is the number of pixels in the prediction domain (Legates and McCabe, 1999; Grecu and Krajewski, 2000).
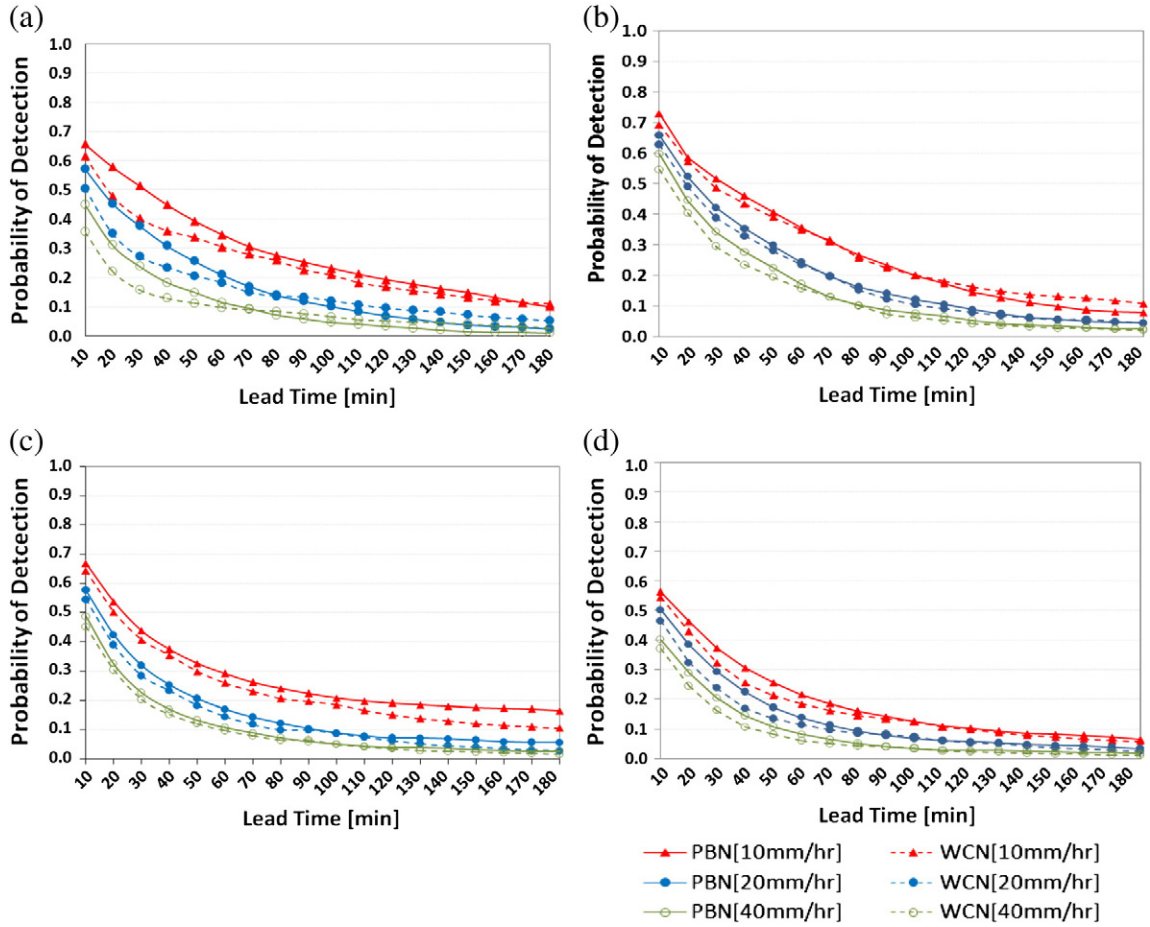
Fig. 12. Probability of Detection (POD) for both PBN and WCN for four events, 10, 20, and 40 [mm/hr] thresholds: (a) Storm 1, (b) Storm 2, (c) Storm 3, and (d) Storm 4, in which the larger value represents better prediction.

The coefficient of efficiency E is defined as:

$$E = 1 - \frac{\sum_{i=1}^{N} (O_i - F_i)^2}{\sum_{i=1}^{N} (O_i - P_i)^2} \qquad (12)$$

where P is the indicator of the persistency in which there is no prediction (last available imagery before prediction; e.g., time $= t$). E will be between 0–1, where a value of 1 is a perfect prediction. A larger E indicates a better agreement between observation and prediction. However, E will be zero in the event that the prediction has less skill than the persistency. This means that the observations are described better by the persistency algorithms rather than by forecasts (Legates and McCabe, 1999).

POD and FAR are defined as:

$$POD = \frac{n_h}{n_f + n_h} \qquad (13)$$

$$FAR = \frac{n_{fa}}{n_{fa} + n_h} \qquad (14)$$

where n_h represents the number of hits, n_f is the number of failures, and n_{fa} represents the number of false alarms. Grecu and Krajewski (2000) stated that POD and FAR are better metrics for pattern matching. POD shows the ability of the nowcasting algorithm in prediction of rainy/non-rainy pixels, based upon predefined thresholds. FAR indicates places in which the storm is predicted while there is no storm. Hogan et al. (2009) also indicated that POD and FAR have limitations in characterizing forecasting skill. Stephenson (2000) represents the Odds ratio as a complementary verification measure.

$$Odds \quad ratio = \frac{n_h \times n_{cn}}{n_{fa} \times n_f} \qquad (15)$$

where n_{cn} is the number of correct negative. The Odds ratio has range between 0 to ∞, that the greater has the better skill (Stephenson, 2000). The current study uses the logarithm of the Odds ratio.

In Table 2, the concepts of hit, false alarm, and failure are described.

An important issue to point out is that pixel-to-pixel based measures are not always accurate in terms of their ability to capture the correspondence between forecasts and
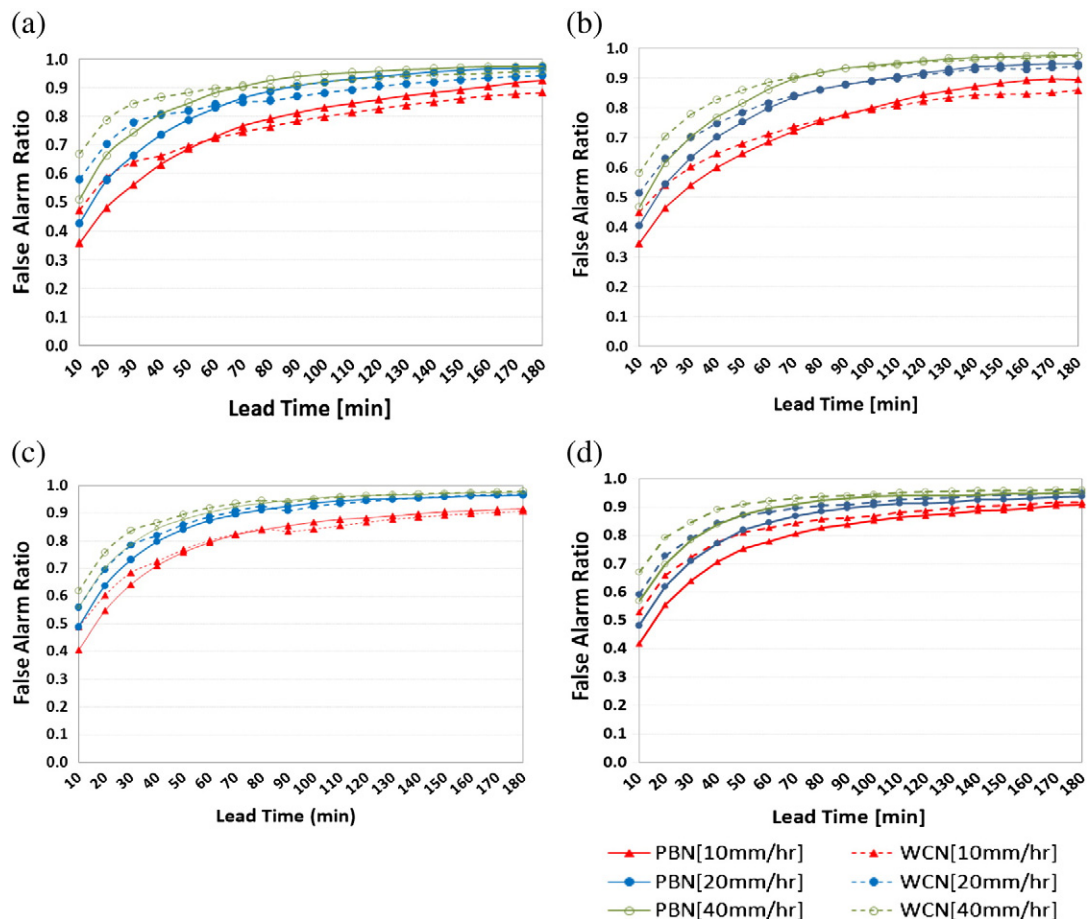
Fig. 13. False-Alarm Ratio (FAR), PBN, and WCN for four events, 10, 20, and 40 [mm/hr] thresholds: (a) Storm 1, (b) Storm 2, (c) Storm 3, and (d) Storm 4, in which the smaller value predicts better.

the verification fields at the pixel level. In other words, if a model forecast at the pixel level does not compare well with the available observation, it does not necessarily mean that the performance is poor. This is especially the case when the objective is to evaluate the predicted storm's position, along with its severity/intensity (i.e., precipitation rate) in a dynamic mode when storms evolve and move very rapidly. For this reason, other verification measures capable of assessing the storms as evolving objects (as opposed to pixel-to-pixel) are required.

The scenario represented in Fig. 6 is intended to demonstrate the complimentary role of both verification methods in the case of application of the PBN and WCN algorithms to predict a thunderstorm (event 1). This storm, as captured by radar observations (Q2), has a number of high-rainfall cores in which accurate prediction of their locations can be very challenging. As previously mentioned, WCN relies on the application of storm segmentation along with an object-based tracking algorithm that may overestimate or underestimate storm advection. Fig. 6 compares the prediction capability of both PBN (Fig. 6 b.c) and WCN (Fig. 6 d.e) for 30 min and 5- and 20-mm/hr rainfall thresholds. Comparing Fig. 6b–e and also Table 3 shows that the PBN algorithm has predicted the storm more accurately, particularly for higher rates of rainfall (i.e., 20 mm/hr, in this

case). To capture these subtle, yet important differences, it is necessary to apply measures capable of verifying the skill of the nowcasting algorithms in detecting how storms (treated as "objects") correspond to observations. Following is a brief description of an object-based verification measure which is intended to overcome the shortcomings of the pixel-based verification measures for such situations as presented in Fig. 6.

4.3.2. Object-based verification method

Several classes of object-based verification methods have been introduced (Ebert, 2009; Wernli et al., 2009). In this study, we implement an object-based verification metric that illustrates how two predicted and observed storms are either close or overlapped with each other. To calculate the metric, it is necessary to set some thresholds to segment the storms of various intensity levels; no filtering or image modification is needed (Davis et al., 2006; Zhu et al., 2011).

The evaluation index is calculated by the weighted combination of two metrics between the observed object "*A*" and predicted object "*B*", as follows (Zhu et al., 2011):

$$metr_v(A, B) = \lambda_1 dist_{OV}(A, B) + \lambda_2 dist_{DV}(A, B) \quad (16)$$

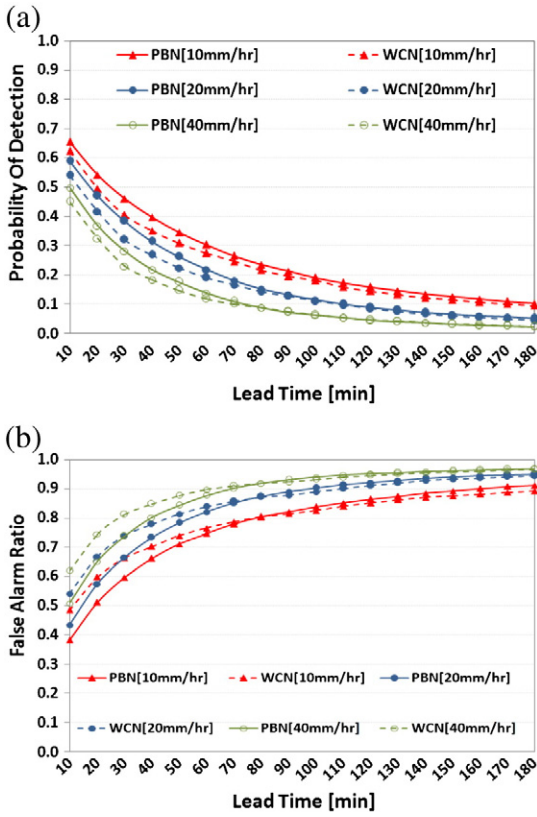in which $dist_{OV}$ and $dist_{DV}$ are overlapped and observation-

Fig. 14. Average of ten storms, (a) Probability of Detection (POD) vs. lead time [min]; (b) False-Alarm Ratio (FAR) vs. lead time [min], for thresholds 10, 20, and 40 [mm/hr].

based distances, respectively; λ_1, λ_2 are weighting factors, which are set to 0.5 for λ_1 and λ_2. Fig. 7 illustrates the metric definition.

$$dist_{OV}(A,B) = \sqrt{\sum_{\forall i}\sum_{\forall j}\left(a_{ij}-b_{ij}\right)^2} \qquad (17)$$

where a_{ij}, b_{ij} are binary variables related to each pixel of sets A and B; for example, a_{ij} is 1 if the pixel ij is a member of A and 0 if not. The pixel ij is in the set A if it has a value greater than a specified threshold. The overlapping distance is the root mean square error based on a binary field.

The $dist_{ob}$ is the average distance for every single pixel of observation to the predicted set A:

$$dist_{ob}(O,A) = \begin{cases} \dfrac{1}{N(O)}\displaystyle\sum_{i=1}^{N(O)} m_{oA}(o_i,A) & if \quad N(O).N(A)\neq 0 \\ D \quad if \;\; N(O)=0 \quad or \quad N(A)=0 \end{cases} \qquad (18)$$

where m_{oA} is the shortest Euclidean distance between point o_i of the observation pixel to object A. $N(O)$ and $N(A)$ are the number of pixels in both sets. D is a number greater than the maximum possible distance. The upper bound will be applied when the observation or the forecast field is empty. Following Eq. (19), the observation-based distance will be set as:

$$dist_{DV}(A,B) = |dist_{ob}(O,A)-dist_{ob}(O,B)| \qquad (19)$$

In the metric for verification between two objects, observation O and forecast A, one of the $dist_{DV}$ drops away. The metric can be applied simply as (Zhu et al., 2011):

$$metr_v(O,A) = \lambda_1 dist_{OV}(O,A) + \lambda_2 dist_{ob}(O,A) \qquad (20)$$

The unit of the distances is in pixel. It may be used in km based on each pixel dimension.

4.3.3. Discussion of pixel-to-pixel comparisons

The comparisons of PBN vs. the WCN and PER models and observations for the four measures (C, E, POD, and FAR) are displayed in Figs. 8–14. According to Figs. 8, 9, and 10, PBN shows improved performance for shorter lead time, and for longer lead time (~120–150 min) WCN and PBN perform in average the same. Figs. 8 and 9 present the comparison results for C and E measures for the four highlighted events, respectively. As observed from Figs. 8 and 9, PBN performance in the first 80–90 min is consistently better than WCN and is especially noticeable for storms #1 and #3.

Fig. 10 shows both C and E averaged over all ten events listed in Table 1. Comparing with other algorithm results, a correlation coefficient threshold = 0.15 is set. The PBN algorithm shows better performance than WCN when compared against radar observation for the first 90 min. According to Germann et al. (2006) the scale dependency is an important factor in nowcasting skill. Usually small-scale features in the precipitation field have short lifetime. Similarly, the current case studies are dominated with small-scale short lifetime features. This is one of the reasons that the forecasting skill relatively drops after a few minutes.

Fig. 11 presents the averaged correlation coefficients of all ten events for +30 and +60 min predictions vs. different spatial resolutions. The coarser resolution (2, 4, 8, 16, 32 km) shows better prediction skill. However, the coarser resolutions might not be able to predict smaller-scale thunderstorms.

The POD of the PBN and WCN algorithms for different rainfall thresholds of four selected events is given in Fig. 12. As evident from this figure, in general, PBN is more skillful in the first 70–90 min; beyond 90–100 min, the skills of both algorithms are relatively the same.

Fig. 13 illustrates the accuracy of prediction in terms of FAR. In general, the same conclusion as in Fig. 12 can be drawn about the performance of PBN when compared against WCN. Figs. 12 and 13 demonstrate that the proposed PBN algorithm has promising results for severe storm events. Fig. 14 illustrates POD and FAR for all ten storms averaged vs. lead time. Assuming a POD threshold of about 0.1 (10%) and rain-intensity thresholds of 10, 20, and 40 mm/hr, PBN provides promising predictions in the first 180, 120, and 80 min, respectively. This is more or less consistent with previously mentioned metrics that the PBN algorithm is reliable for the first 1–2 hr.

Fig. 15 also shows the logarithms of Odds ratios for four events that indicate the PBN algorithm has promising performance in different rain-intensity thresholds (10, 20, and 40 mm/hr).

4.3.4. Discussion of object-based metric comparisons

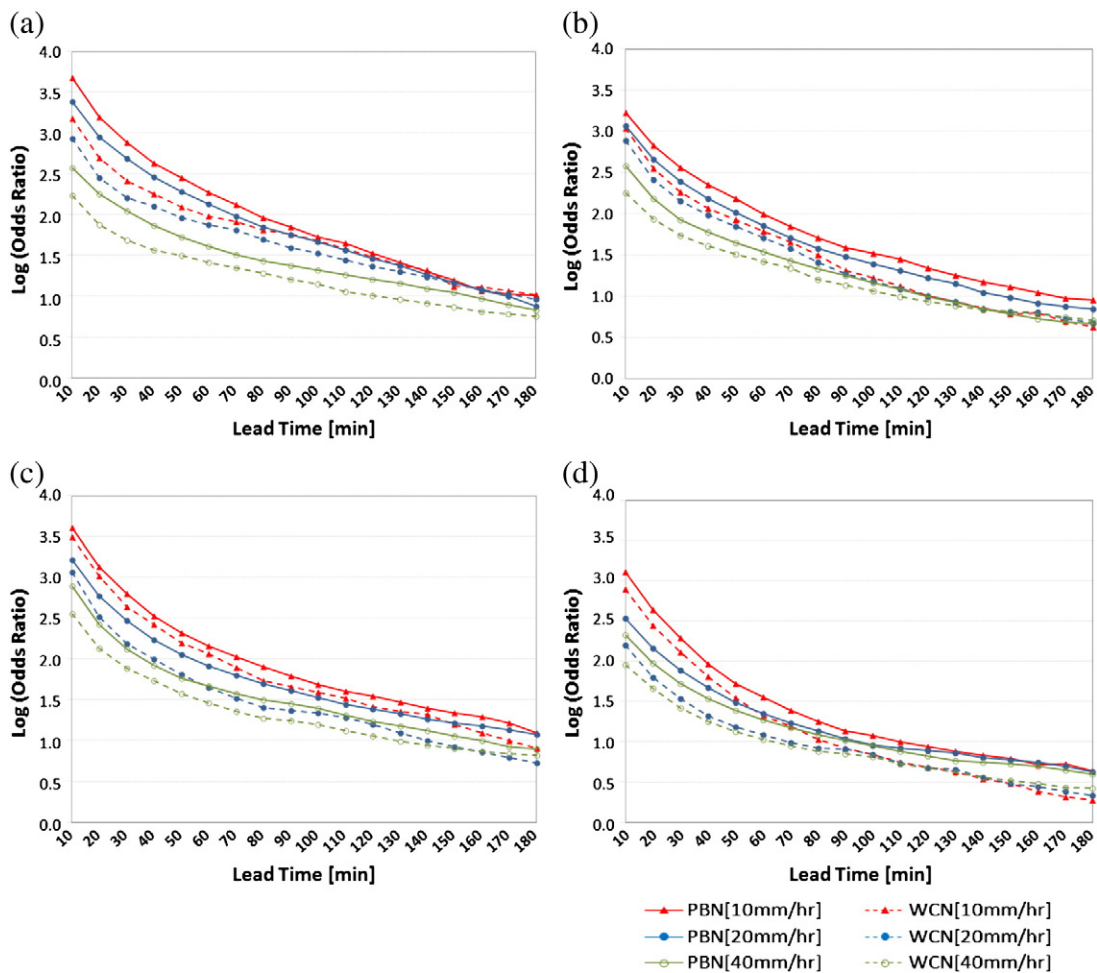The comparisons of PBN vs. the WCN and PER models and observations using the object-based verification metric method

Fig. 15. Logarithm of Odds ratio for both PBN and WCN for four events, 10, 20, and 40 [mm/hr] thresholds: (a) Storm 1, (b) Storm 2, (c) Storm 3, and (d) Storm 4, in which the larger value represents better prediction.

are displayed in Figs. 16 and 17. As evident from the results, PBN shows better performance for the different cases. Fig. 16 gives the normalized object-based verification metric vs. lead time for the four selected events and for all three algorithms. Results reveal that PBN maximizes predictability of storms as compared to PER and WCN in all cases, except storm #3 (Fig. 16c), which is a quasi-stationary storm. It is also encouraging that the PBN algorithm outperforms other algorithms, particularly as the rainfall thresholds increase from 10 to 40 mm/hr. In higher rainfall rates (threshold = 20, or 40 mm/hr), there is a greater gap between PBN and WCN. The PBN is able to predict high-rainfall storms more accurately.

Fig. 17 displays the overall verification results using the object-based verification metric for the average of all ten thunderstorms. In order to generalize the findings with respect to the forecast capability of PBN as a function of storm intensity, two metric thresholds were chosen and tested. For relatively light-rainfall rates (up to 10 mm/hr) and values of the metric up to the threshold = 0.2, the PBN algorithm appears to give better performance in the first

60 min. In relatively heavier-rainfall rates (up to 40 mm/hr), the object-based verification metric values up to the threshold = 0.35 can be selected, which suggests that the forecast made by PBN is reliable up to 30 min.

5. Summary and Conclusions

In this manuscript, we introduce a new nowcasting algorithm named Pixel-Based Nowcasting (PBN) to improve the predictability of severe thunderstorms. The proposed PBN algorithm is particularly suitable for very short-duration forecasts useful for hydrological modeling applications, such as flash-flood forecasting. In testing the PBN prediction capabilities, ten severe storms were selected for their features, including relatively short lifetime, smaller-scale, damaging winds, and rainfall. The performance of PBN was compared against two other models, namely the WCN and PER algorithms. Two verification methods, pixel-based and object-based, were employed to evaluate different aspects of each algorithm as compared to radar observations.
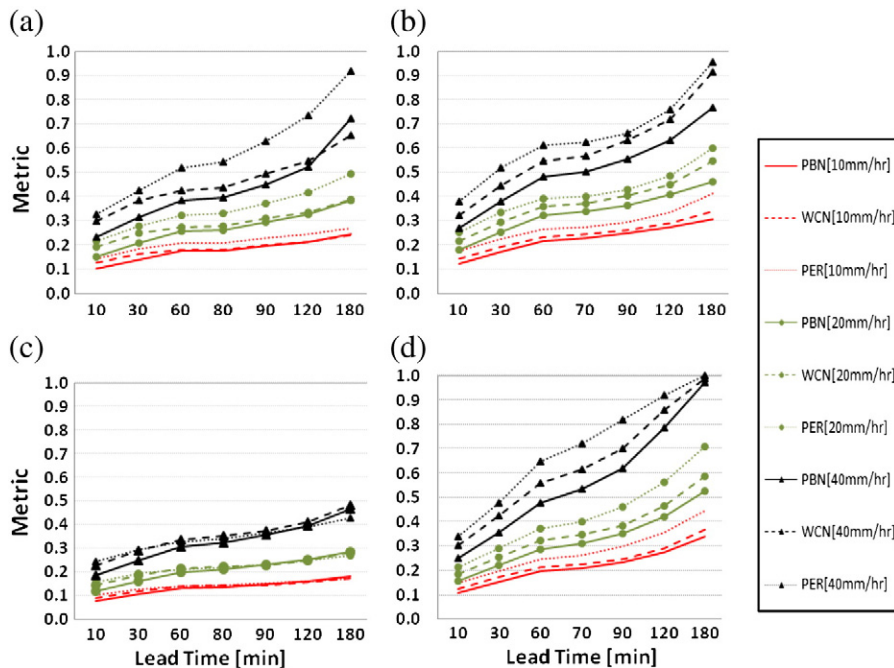
Fig. 16. Metric vs. lead time for different rainfall thresholds: 10, 20, and 40 [mm/hr]: (a) Storm 1, (b) Storm 2, (c) Storm 3, and (d) Storm 4, in which the better prediction has a smaller error metric.

The main conclusion from this research is that PBN shows superior performance over the other two models examined in this study. Following is a summary of the more specific conclusions:

- The pixel-based verification parameters justify the applicability of the proposed PBN model in the first ~90 min for forecasts of thunderstorms.
- The object-based verification metric shows that the PBN algorithm provides promising performance in nowcasting both light- and heavy-rainfall storms. Based on this study, PBN shows promising performance in nowcasting intense storms in the first 30 min. These events might be associated with catastrophic events (e.g., tornados), for which it is very important to accurately predict in the short term.

Fig. 17. Object-based metric verification for the average of all ten thunderstorms vs. lead time; 10, 20, and 40 [mm/hr] rainfall thresholds have been tested. In light rainfall (the 10 mm/hr), the difference between WCN and PBN is less than the difference in high rainfall (20, 40 mm/hr). The better prediction has a smaller error metric.

- Given the object-based verification metric, the difference between PBN and comparisons algorithms in severe rainfall is more than lighter rainfall, which means that the algorithm may outperform other nowcasting techniques, particularly in more severe events.

Acknowledgments

References

Austin, G.L., Bellon, A., 1974. The use of digital weather records for short-term precipitation forecasting. Q. J. R. Meteorol. Soc. 100, 658–664.

Austin, G.L., Bellon, A., Dionne, P., Roch, M., 1987. 1987: On the interaction between radar and satellite image nowcasting systems and mesoscale numerical models. Proceedings, Symposium on Mesoscale Analysis and Forecasting, Vancouver, ESA SP-282, pp. 225–228.

Behrangi, A., Imam, B., Hsu, K.L., Sorooshian, S., Bellerby, T., Huffman, G., 2010. REFAME: Rain Estimation Using Forward-Adjusted Advection of Microwave Estimates. J. Hydrometeorol. 11, 1305–1321.

Bellerby, T., 2006. High-resolution 2-D cloud-top advection from geostationary satellite imagery. IEEE Trans. Geosci. Remote. Sens. 44, 3639–3648.
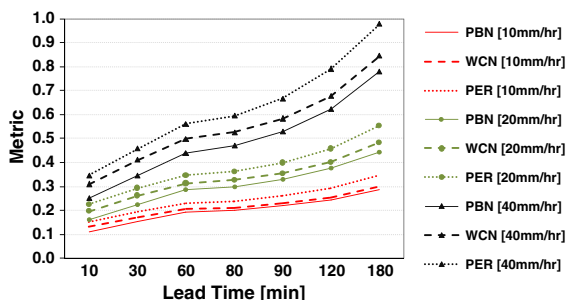
Benjamin, S.G., Devenyi, D., Weygandt, S.S., Brundage, K.J., Brown, J.M., Grell, G.A., Kim, D., Schwartz, B.E., Smirnova, T.G., Smith, T.L., Manikin, G.S., 2004. An hourly assimilation-forecast cycle: The RUC. Mon. Weather Rev. 132, 495–518.

Benjamin, S.G., Smirnova, T.G., Weygandt, S.S., Hu, M., Sahm, S.R., Jamison, B.D., Wolfson, M.M., Pinto, J.O., 2009. The HRRR 3-km storm resolving, radar-initialized, hourly updated forecasts for air traffic management. AMS Aviation, Range and Aerospace Meteorology Special Symposium on Weather-Air Traffic Management Integration, Phoenix, AZ.

Bergen, J.R., Anandan, P., Hanna, K.J., Hingorani, R., 1992. Hierarchical model-based motion estimation. Proc. ECCV, Italy, pp. 237–252.

Bowler, N., Pierce, C., Seed, A., 2004. Development of a precipitation nowcasting algorithm based upon optical flow techniques. J. Hydrol. 288, 74–91.

Davis, C., Brown, B., Bullock, R., 2006. Object-based verification of precipitation forecasts. Part I: Methodology and application to meso-scale rain areas. Mon. Weather Rev. 134 (7), 1772–1784.

Dixon, M., Wiener, G., 1993. TITAN: Thunderstorm Identification, Tracking, Analysis and Nowcasting—A radar-based methodology. J. Atmos. Oceanic Technol. 10, 785–797.

Ebert, E., 2009. Neighborhood verification: A strategy for rewarding close forecasts. J. Weather Forecast 24 (6), 1498–1510.

Ganguly, A.R., Bras, R.L., 2003. Distributed quantitative precipitation forecasting using information from radar and Numerical Weather Prediction models. J. Hydrometeorol. 4 (6), 1168–1180.

Germann, U., Zawadzki, I., 2002. Scale-dependence of the predictability of precipitation from continental radar images. Part I: Description of the methodology. Mon. Weather Rev. 130 (12), http://dx.doi.org/10.1175/1520-0493(2002)130.

Germann, U., Zawadzki, I., 2004. Scale-dependence of the predictability of precipitation from continental radar images. Part II: Probability forecasts. J. Appl. Meteorol. 43 (1), 74–89.

Germann, U., Zawadzki, I., Turner, B., 2006. Predictability of precipitation from continental radar images. Part IV: Limits to prediction. J. Atmos. Sci. 63, 2092–2108.

Golding, B.W., 1998. Nimrod: A system for generating automated very short range forecasts. Meteorol. Appl. 5 (1), 1–16.

Grecu, M., Krajewski, W.F., 2000. A large-sample investigation of statistical procedures for radar-based short-term quantitative precipitation forecasting. J. Hydrol. 239, 69–84.

Hogan, R., O'Connor, E., Illingworth, A., 2009. Verification of cloud–fraction forecasts. Q. J. R. Meteorol. Soc. 135, 1494–1511.

Johnson, J.T., MacKeen, P.L., Witt, A., Mitchell, E.D., Stumpf, G.J., Eilts, M.D., Thomas, K.W., 1998. The Storm Cell Identification and Tracking (SCIT) algorithm: An enhanced WSR-88D algorithm. Weather. Forecast. 13, 263–276.

Lakshmanan, V., Fritz, A., Smith, T., Hondl, K., Stumpf, G.J., 2007. An automated technique to quality control radar reflectivity data. J. Appl. Meteorol. Climatol. 46, 288–305.

Lakshmanan, V., Hondl, K., Rabin, R., 2009. An efficient, general-purpose technique for identifying storm cells in geospatial images. J. Atmos. Oceanic Technol. 26, 523–537.

Laroche, S., Zawadzki, I., 1995. Retrievals of horizontal winds from single Doppler clearair data by methods of cross correlation and variational analysis. J. Atmos. Oceanic Technol. 12, 721–738.

Leese, J., Novak, C.S., Clark, B.B., 1971. An automated technique for obtaining cloud motion from geosynchronous satellite data using cross-correlation. J. Appl. Meteorol. 10 (1), 118–132.

Legates, D.R., McCabe Jr., G.J., 1999. Evaluating the use of "goodness-of-fit" measures in hydrologic and hydroclimatic model validation. Water Resour. Res. 35, 233–241.

Li, L., Schmid, W., Joss, J., 1995. Nowcasting of Motion and Growth of Precipitation with Radar over a Complex Orography. J. Appl. Meteorol. 34, 1286–1300.

Liang, Q., Feng, Y., Deng, W., Hu, S., Huang, Y., Zeng, Q., Chen, Z., 2010. A composite approach of radar echo extrapolation based on TREC vectors in combination with model-predicted winds. Adv. Atmos. Sci. 27 (5), 1119–1130, http://dx.doi.org/10.1007/s00376-009-9093-4.

Liguori, S., Rico-Ramirez, M.A., Schellart, A.N.A., Saul, A.J., 2012. Using probabilistic radar rainfall nowcasts and NWP forecasts for flow prediction in urban catchments. J. Atmos. Res. 103, 80–95.

Lin, C., Vasic, S., Ki Lambi, A., Turner, B., Zawadzki, I., 2005. Precipitation forecasting skill of numerical weather prediction models and radar nowcasts. Geophys. Res. Lett. 32, L14801, http://dx.doi.org/10.1029/2005GL023451.

Montanari, L., Montanari, A., Toth, E., 2006. A comparison and uncertainty assessment of system analysis techniques for short-term quantitative precipitation nowcasting based on radar images. J. Geophys. Res. 111, D14111, http://dx.doi.org/10.1029/2005JD006729 (12 pp.).

Mueller, C., Saxen, T., Roberts, R., Wilson, J., Betancourt, T., Dettling, S., Oien, N., Yee, J., 2003. NCAR auto-nowcast system. Weather. Forecast. 18 (4), 545–561.

Pegram, G.G.S., Clothier, A.N., 2001a. Downscaling rainfields in space and time, using the string of beads model in time series mode. Hydrol. Earth Syst. Sci. 5 (2), 175–186.

Pegram, G.G.S., Clothier, A.N., 2001b. High resolution space-time modelling of rainfall: The "String of Beads" model. J. Hydrol. 241 (1–2), 26–41.

Ridal, M., Lindskog, M., Gustafsson, N., Haase, G., 2010. Optimized advection of radar reflectivities. J. Atmos. Res. 100 (2–3), 213–225.

Seed, A.W., 2003. A dynamic and spatial scaling approach to advection forecasting. J. Appl. Meteorol. 42, 381–388.

Smythe, G.R., Zrnic, D.S., 1983. Correlation analysis of Doppler radar data and retrieval of the horizontal wind. J. Clim. Appl. Meteorol. 22, 297–311.

Sokol, Z., Pesice, P., 2012. Nowcasting of precipitation - advection statistical forecast model (SAM) for the Czech Republic. J. Atmos. Res. 103, 70–79.

Stephenson, D., 2000. Use of the "odds ratio" for diagnosing forecast skill. Weather. Forecast. 15, 221–232.

Toklu, C., Erdem, A.T., Sezan, M.I., Tekalp, A.M., 1996. Tracking motion and intensity variations using hierarchical 2-D mesh modeling for synthetic object transfiguration. Graph. Models Image Process. 58 (6), 553–573.

Turner, B., Zawadzki, I., Germann, U., 2004. Predictability of precipitation from continental radar images. Part III: Operational nowcasting implementation (MAPLE). J. Appl. Meteorol. 43, 231–248.

Tuttle, J.D., Foote, G.B., 1990. Determination of the boundary layer airflow from a single Doppler radar. J. Atmos. Oceanic Technol. 7, 218–232.

Vasiloff, S.V., Seo, D.J., Howard, K.W., Zhang, J., Kitzmiller, D.H., Mullusky, M.G., Krajewski, W.F., Brandes, E.A., Rabin, R.M., Berkowitz, D.S., Brooks, H.E., McGinley, J.A., Kuligowski, R.J., Brown, B.G., 2007. Improving QPE and very short term QPF: An initiative for a community-wide integrated approach. Bull. Am. Meteorol. Soc. 88, 1899–1911.

Vieux, B., Vieux, J., 2005. Statistical evaluation of a radar rainfall system for sewer system management. J. Atmos. Res. 77 (1–4), 322–336.

Vila, D.A., Machado, L.A.T., Laurent, H., Velasco, I., 2008. Forecast and Tracking the Evolution of Cloud Clusters (ForTraCC) using satellite infrared imagery: Methodology and validation. Weather. Forecast. 23, 233–245.

Wang, W., Lee, O., 1996. Use of two-dimensional mesh structures for video coding: Part 1—The synthesis problem: Mesh-based function approximation and mapping. IEEE Trans. Circuits Syst. Video Technol. 8 (6), 243–252.

Wernli, H., Hofmann, C., Zimmer, M., 2009. Spatial forecast verification methods intercomparison project–application of the SAL technique. Weather. Forecast. 24, 1472–1484.

Wilson, J.E., Ebert, E., Saxen, T.R., Roberts, R.D., Mueller, C.K., Sleigh, M., Pierce, C.E., Seed, A., 2004. Sydney 2000 Forecast Demonstration Project: Convective storm nowcasting. Weather. Forecast. 19, 131–150.

Wolfson, M.M., Dupree, W.J., Rasmussen, R., Steiner, M., Benjamin, S., Weygandt, S., 2008. Consolidated Storm Prediction for Aviation (CoSPA). American Meteorology Society 13th Conference on Aviation, Range, and Aerospace Meteorology, New Orleans, LA.

Zahraei, A., Hsu, K., Sorooshian, S., 2011a. Short-term quantitative precipitation forecasting using satellite and radar information. Ph.D., Dissertation, University of California, Irvine, CA.

Zahraei, A., Hsu, K., Sorooshian, S., Behrangi, A., 2011b. Advection-based short-term quantitative precipitation forecasting algorithm. American Geophysical Union Fall Meeting, San Francisco, CA. http://www.agu.org/cgi-bin/SFgate/SFgate?language=English&verbose=0&listenv=table&application=fm11&convert=&converthl=&refinequery=&formintern=&formextern=&transquery=advection-based%20short-term%20quantitativeprecipitation%20forecasting%20algorithm&_lines=&multiple=0&descriptor=%2fdata%2fepubs%2fwais%2findexes%2ffm11%2ffm11%7c1000%7c3240%7cAdvection-based%20Short-Term%20Quantitative%20Precipitation%20Forecasting%20Algorithms%20Using%20Radar%20and%20Satellite%20Information%7cHTML%7clocalhost:0%7c%2fdata%2fepubs%2fwais%2findexes%2ffm11%2ffm11%7c31518932%2031522172%20%2fdata%2f%2fepubs%2fwais%2fdata%2fm11%2ffm11.txt.

Zahraei, A., Hsu, K., Sorooshian, S., Behrangi, A., 2012. Short-Term Severe Storms Forecasting Using An Object-Based Tracking Technique. AMS 18th Conference on Satellite Meteorology, Oceanography and Climatology, New Orleans, LA. https://ams.confex.com/ams/92Annual/webprogram/Paper201880.html.

Zahraei, A., Hsu, K., Sorooshian, S., Gourley, J.J., Hong, Y., V., Behrangi, A., submitted for publication. Short-term quantitative precipitation forecasting: Short-Term Quantitative Precipitation Forecasting Using an Object-Based Approach. J. Hydrol.

Zhu, M., Lakshmanan, V., Zhang, P., Hong, Y., Cheng, K., Chen, S., 2011. Spatial verification, using a true metric. J. Atmos. Res. 102 (4), 408–419.